Investigation on wing resistance of a pile with a wing plate based on centrifuge model tests

Hiroko Suzuki[*1], Kohei Urabe[*2], Kohji Tokimatsu[*2] & Yoshiharu Asaka[*3]
[*1] *Chiba Institute of Technology, Chiba, Japan*
[*2] *Tokyo Institute of Technology, Tokyo, Japan*
[*3] *Shimizu Corporation, Tokyo, Japan*

ABSTRACT
Cyclic vertical loading due to the overturning moment of structures may reduce frictional resistance of piles, which affects their bearing capacity and pull-out resistance. This decrease in frictional resistance may tilt a structure. To estimate bearing capacity and pull-out resistance of piles during cyclic loading, vertical loading tests were conducted on a pile with a wing plate near its tip and the resistance of a wing (wing resistance) was determined to be effective against pull-out loading. The objective of this study is to further investigate the mechanism of the wing resistance development. Vertical loading tests were conducted on piles with or without a wing plate near the tip under a centrifugal acceleration of 30 g. Monotonic and cyclic loading tests on a pile penetrating into a dry sand deposit were performed under a displacement-controlled condition. The test results and discussions show the following. 1) Shaft friction after reaching its ultimate value during cyclic loading, decreases to approximately 50 % in compression and approximately 20 % in tension with respect to that in monotonic loading with the same displacement. 2) Wing piles have high compression and tension resistances. The tensile resistance of wing piles with a wing ratio of approximately 1.5 decreases significantly with increasing cyclic vertical displacement. However, the tensile resistance of wing piles with a wing ratio of approximately 2.0 does not show a significant decrease. 3) The wing resistance is estimated according to the model assuming that the earth pressure coefficient above a wing plate changes to that at the passive state. The estimated wing resistance is generally in agreement with the observed ones.

1 INTRODUCTION

During earthquake, piles supporting structures suffer cyclic vertical loading because of the overturning moment from the structure. Cyclic vertical loading may reduce frictional resistance of piles; this affects the bearing capacity and uplift resistance. This decrease in frictional resistance may cause permanent tilt of a structure. Urabe et al. (2015) and Suzuki et al. (2013, 2014) conducted vertical loading tests on a pile with a wing plate near its tip under a centrifugal acceleration of 30 g. The results showed that the resistance of a wing (wing resistance) was effective after the shaft friction decreased due to cyclic loading. As only the shaft friction acts against pull-out loading in the case of a straight pile, the presence of a wing is of great advantage to the uplift resistance. However, the specific mechanism of wing resistance development has not been thoroughly examined. The objective of the current study is to further investigate the wing resistance based on the centrifuge model tests.

2 CENTRIFUGE MODEL TESTS

Centrifuge model tests were conducted on one straight pile and four wing piles under centrifugal acceleration of 30 g and the test models were on a scale of 1-30 in length. Figure 1 illustrates a test model. A single pile was set with an embedment depth of 250 mm in dry Toyoura sand (e_{max} = 0.982, e_{min} = 0.604) in a cylindrical rigid box of 500 mm height. The sand was air-pluviated with a constant fall height to form a uniform layer. When the sand layer reached the designated height (160 mm), the model pile with a penetration depth of 10 mm was set into it. Next, the remaining layer was air-pluviated to a height of 400 mm. The sand layer had a density of 1.62 g/cm^3, corresponding to a relative density of 90 % -96 %.

In reality, a pile with a wing plate is installed using screw-piling methods. Installation methods significantly affect the generation of shaft friction (White and Lehane, 2004), and the different installation methods might cause difference in the magnitude of shaft friction. However, discussion on trends in shaft friction during cyclic is thought to be useful.

Figure 2 shows five model piles and Table 1 lists their characteristics. Each pile has a different shaft diameter D and wing diameter D_w. Pile IDs are defined by shaft diameter, pile type, and wing ratio D_w/D. The model piles were made of stainless steel pipes. Pile-2S did not have a wing plate. The other piles comprised a wing plate made of stainless steel that was welded to the pipe's tip. To increase the shaft friction, dry Toyoura sand was pasted on the surface of each pile. Each pile had strain gauges on the inner surface of the pipe at seven or eight depths and a load cell at the tip. The end condition affects the capacity of piles, as shown in the previous studies (e.g., Schneider et al., 2008). In the current study, as a load cell was attached to the tip, every pile had the close-end condition.

To perform vertical loading, a hydraulic actuator was joined with a pile head. Table 2 lists the tests performed and Figure 3 shows the loading histories. In monotonic loading tests, piles were pushed or pulled to the designated displacement (Figure 3(a)). In cyclic loading

tests, the loading displacement amplitude was gradually increased in four steps (±0.217, 1.09, 2.17, and 3.26 mm) and repeated three times in each step (Figure 3(b)). The four steps are corresponding to 1 %, 5 %, 10 %, and 15 % of 21.7 mm, which is the shaft diameter of piles 2S, 2W1.5 and 2W2.0.

The tests recorded the vertical load and displacement at the pile head, the tip resistance, and the axial strains at seven or eight depths of the piles. To investigate factors influencing the wing resistance generation, an additional test was conducted for Case 2W2.0_St, in which earth pressure transducers were installed in the soil around a pile. Vertical and horizontal earth pressures were measured at six depths, as shown in Figure 1. The relation of load and displacement in the two tests for Case 2W2.0_St showed a similar trend, confirming that the presence of earth pressure transducers do not affect the results.

Figure 4 shows the forces acting on the pile; these are defined by the following equations:

$$Q_c = R_p + R_{fc} + R_{wc} \quad \text{< in pushing direction>} \quad (1)$$

$$Q_t = R_{ft} + R_{wt} \quad \text{< in pulling direction>} \quad (2)$$

where Q_c and Q_t are the pile-head axial force, R_p is the tip resistance, R_{fc} and R_{ft} are the shaft frictions, R_{wc} and R_{wt} are the wing resistances. The subscripts c and t indicate the values in compression (pushing) or tension (pulling), respectively. The shaft friction R_f is estimated from the difference between the pile head axial force Q and the axial force observed at strain gauge SG7. The wing

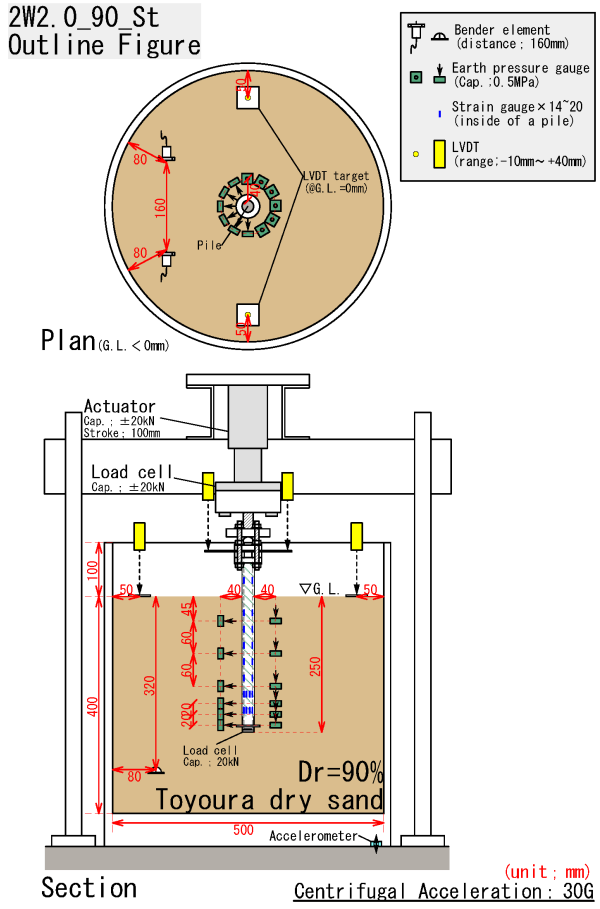

Figure 1. Test model

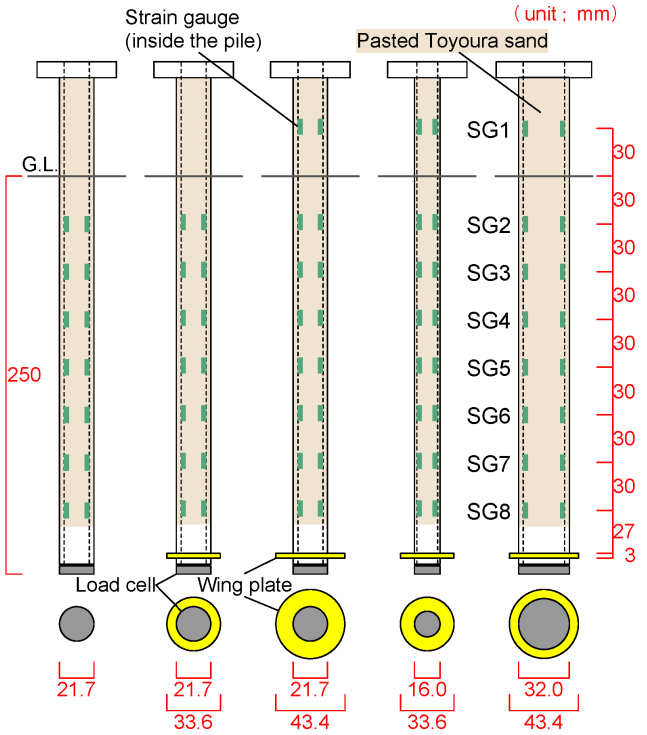

Figure 2. Model piles

Table 1. Characteristics of model piles

ID	Pile type	Shaft diameter D [mm]	Wing diameter D_w [mm]	Wing ratio D_w/D	Wing area A_w [× 10^2mm^2]	Thickness of pile t [mm]
2S	Straight pile S	21.7	-	-	-	3.0
2W1.5	Wing pile W	21.7	33.6	1.5	5.2	3.0
2W2.0		21.7	43.4	2.0	11.1	3.0
1W2.1		16.0	33.6	2.1	6.9	1.5
3W1.4		32.0	43.4	1.4	6.8	3.0

ID of pile models

2W1.5

Shaft diameter: 1 ; 16.0mm, 2 ; 21.7mm, 3 ; 32.0mm
Pile type: S ; Straight pile, W ; Wing pile
Wing ratio

resistance R_w is estimated from the difference between the axial force observed at strain gauge SG7 and tip resistance R_p. As expected, a straight pile has no wing resistance. In this study, positive values represent compression and negative values represent tension. The values in the following part correspond to the values of the prototype scale.

3 BEARING CAPACITIES AND UPLIFT RESISTACE OF PILES

Figures 5-8 show the relations of the pile head displacement with the tip resistance R_p, shaft friction R_f, and wing resistance R_w and pile head axial force Q. The solid lines and broken lines represent the results of cyclic and monotonic loading tests, respectively.

Figure 5 shows that the tip resistance is larger in the cyclic loading tests than in the monotonic loading tests after the amplitude displacement reaches 65.1 mm (2.17 mm in model scale). In addition, it is interesting to note that the tip resistance is generated with the negative displacement when loading shifts from tension to compression. This is probably because the sand might have moved beneath the tip in tension and was compacted by the tip in compression.

Figure 6 shows that the shaft friction in monotonic loading reaches an ultimate value when the displacement is approximately ±30-100 mm, and decreases gradually with increasing displacement. In contrast, during cyclic loading, the shaft friction reaches an ultimate value when the pile head displacement amplitude is approximately ±30 mm, and decreases significantly with increasing displacement. Figure 9 shows distributions of axial force with respect to depth for 1st and 3rd cycles of amplitude of 32.7 mm (1.09 mm in model scale) for Case 2W2.0_Cyc, at which the shaft friction decreases significantly. The difference in axial force for the two cycles is more remarkable in tension than in compression, confirming that the degradation of shaft friction is more significant in tension than in compression. With increasing the number of cycles, the shaft friction in cyclic loading decreases to approximately 50 % in compression and approximately 20 % in tension compared with that in monotonic loading with the same displacement (Figure 6).

The difference in shaft friction between directions might be induced by the difference in soil stress due to shear deformation. Pushing a pile drags down the soil around the pile, and then increases the soil stress; whereas, pulling a pile lifts up the soil, causing the stress around the pile to decrease. As a result, the degradation in shaft friction is significant in tension. In addition, in this study, the same displacement amplitude was applied to

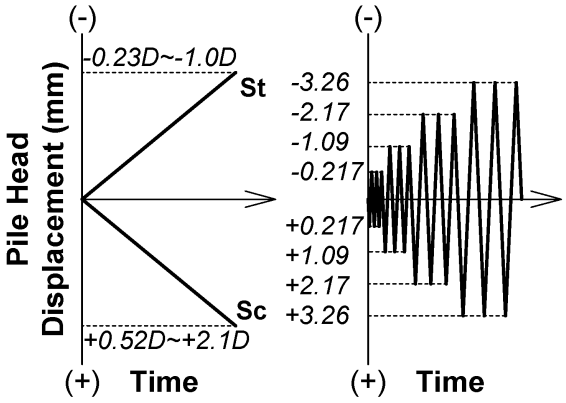

Figure 3. Loading histories

Table 2. Series of loading tests

Case ID	Pile	Loading	Loading displacement*1
2S_Sc	2S	Monotonic compressive loading Sc	+21.7mm (+1.00D)
2W1.5_Sc	2W1.5		+33.6mm (+1.55D)
2W2.0_Sc	2W2.0		+17.5mm (+0.81D)*2
1W2.1_Sc	1W2.1		+33.6mm (+2.10D)
3W1.4_Sc	3W1.4		+16.5mm (+0.52D)*2
2S_St	2S	Monotonic tensile loading St	-21.7mm (-1.00D)
2W1.5_St	2W1.5		-5.0mm (-0.23D)
2W2.0_St	2W2.0		-21.7mm (-1.00D)
1W2.1_St	1W2.1		-16.0mm (-1.00D)
3W1.4_St	3W1.4		-16.0mm (-0.50D)
2S_Cyc	2S	Alternately cyclic vertical loading Cyc	± 0.217mm ⇒± 1.09mm ⇒± 2.17mm ⇒± 3.26mm repeated 3 times in each step
2W1.5_Cyc	2W1.5		
2W2.0_Cyc	2W2.0		
1W2.1_Cyc	1W2.1		
3W1.4_Cyc	3W1.4		

*1…+: Pushing direction, -: Pulling direction
*2…Loaded until the pile head axial force reached the maximam loading capacity of the actuator

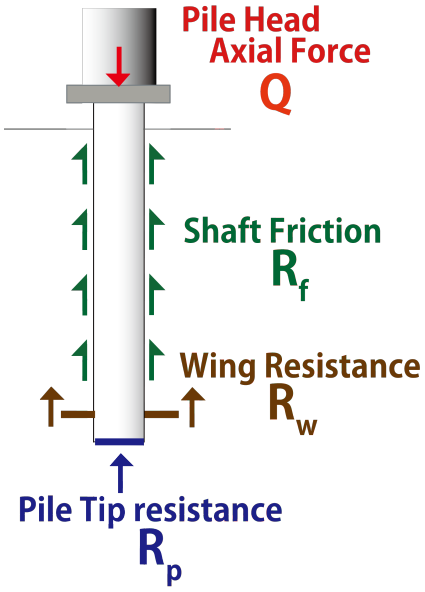

Figure 4. Forces acting on pile

both compression and extension directions under displacement controlled. This might have caused more severe damage to extension resistance, as the degradation of shaft friction during cyclic loading depends on the ratio of amplitude load with respect to the static capacity (Tsuha et al., 2012).

Figure 7 shows that the wing resistance in the pushing direction increases with the loading steps. Similar to the tip resistance, this is because the sand might have moved beneath the wing during tension and compacted during compression. In contrast, in the pulling direction, the wing resistance in the wing piles with a small wing area (Pile-2W1.5, 1W2.1 and 3W1.4) decreases significantly (Figures 7(a), (c), and (d)), while the wing resistance in the wing piles with a large wing area (Pile-2W2.0) does not show significant decrease (Figure 7(b)). This decrease is probably induced by a disturbance and the decrease in soil density above the wing. Both the wing ratio and wing area might have affected the wing resistance during tension.

Figure 8 shows that during compression of the cyclic loading tests, the pile-head axial force *Q* increases as the pile-head displacement amplitude and the number of cycles increase. In contrast, during tension, the pile-head axial force decreases significantly as the pile head displacement amplitude and the number of cycles

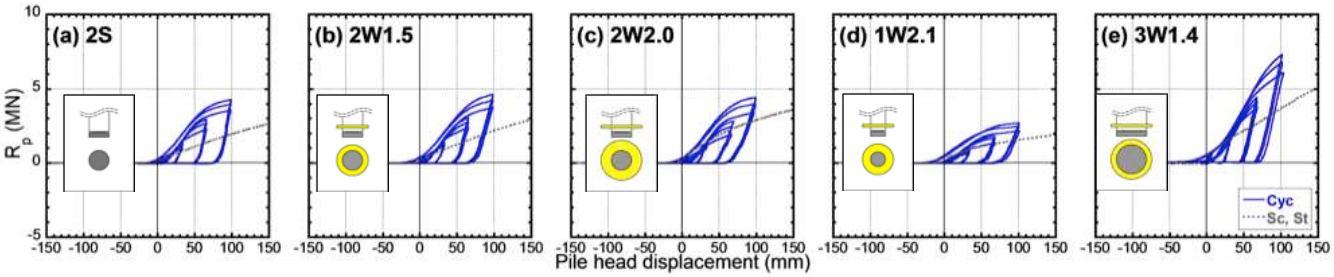

Figure 5. Relationship between tip resistance and pile head displacement

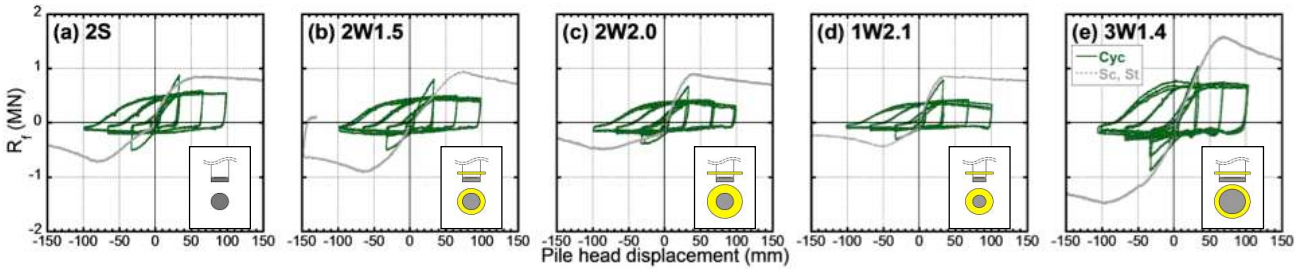

Figure 6. Relationship between shaft friction and pile head displacement

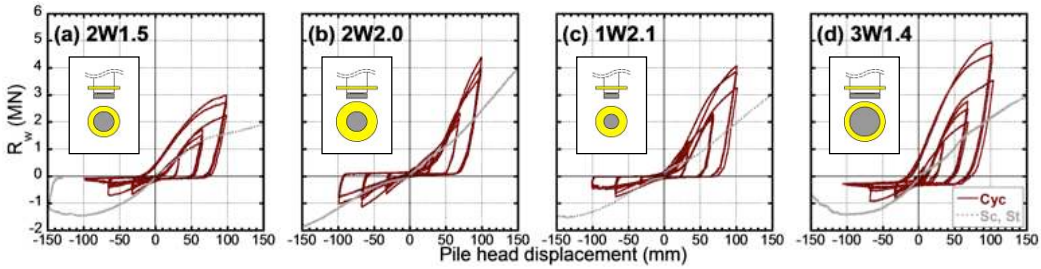

Figure 7. Relationship between wing resistance and pile head displacement

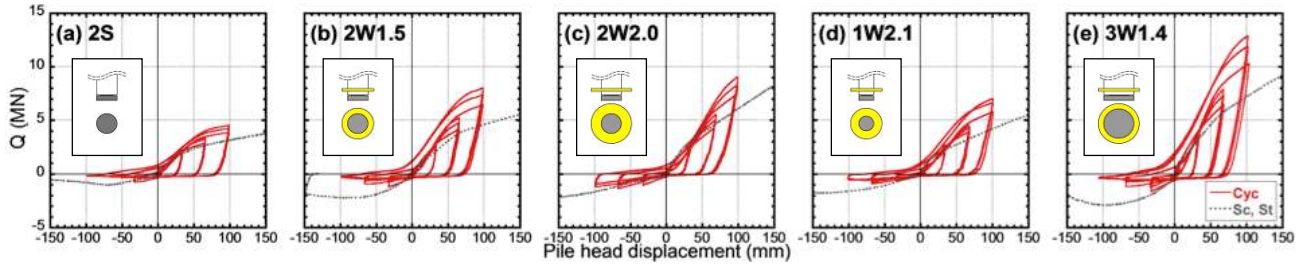

Figure 8. Relationship between pile head axial force and pile head displacement

increase (Figures 8(a), (b), (d), and (e)); however, in Pile-2W2.0 (Figure 8(c)), the wing resistance acts effectively against the vertical force when the shaft friction decreases with cyclic loading.

Figures 10-14 show the relations of the loading step with the tip resistance, shaft friction and wing resistance in cyclic loading (Urabe et al., 2015). It confirms that the tip and wing resistances in compression increase with increasing displacement amplitude and the number of cycles, while the shaft friction in compression and tension and the wing resistance in tension decrease.

4 ESTIMATION OF WING RESISTANCE

As shown in the previous section, wing resistance plays an important role in the tension direction. To estimate the stress state of soil during loading, the earth pressure coefficient is computed from the horizontal and vertical earth pressures measured in soil around a pile. Figure 15 shows the earth pressure coefficient during tension with the pile head displacement for Case 2W2.0_St. The coefficients of earth pressure at rest and passive state, that is, K_0 and K_P, respectively, shown in Figure 15 were estimated based on the assumption that the friction angle is 43° .

Figures 15(a)-(c) and (f) show that the values of earth pressure coefficient are between 0.5 and 1, which almost corresponds to those at rest. In contrast, the earth pressure coefficients at depths of 6.0 and 6.6m increase with the vertical displacement, the value of which increases up to that at the passive state (Figures 15(d) and (e)). This depth is related to that just above the wing plate, suggesting that the coefficient of earth pressure

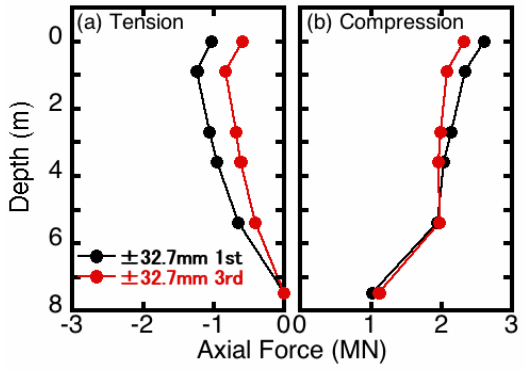

Figure 9. Distributions of axial force with depth

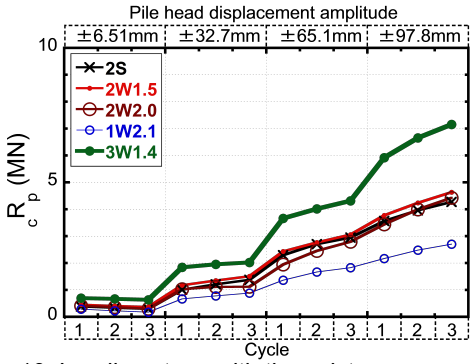

Figure 10. Loading steps with tip resistance

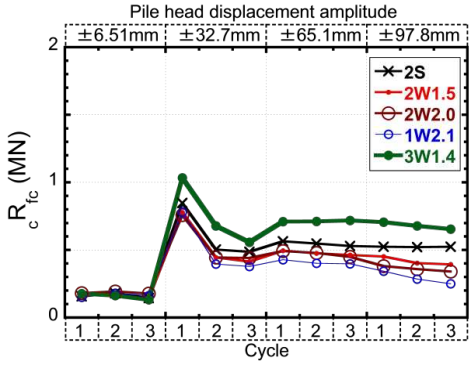

Figure 11. Loading steps with shaft friction in compression

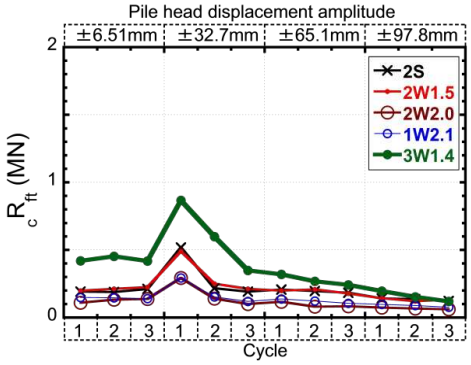

Figure 12. Loading steps with shaft friction in tension

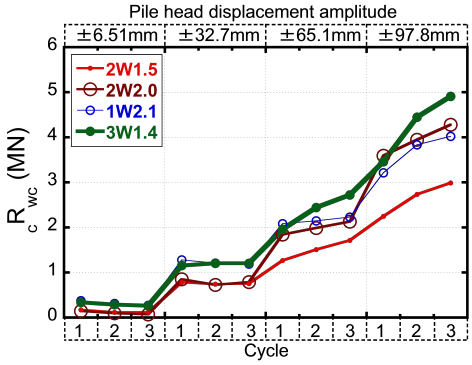

Figure 13. Loading steps with wing resistance in compression

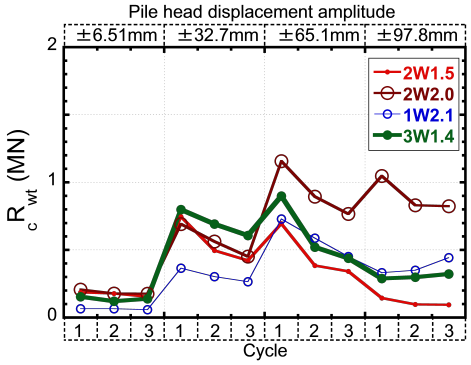

Figure 14. Loading steps with wing resistance in tension

increases because of the uplifting of the wing plate.

To estimate the uplift resistance of deep foundation with a wing, Kanatani and Akino (1983) proposed a model as shown in Figure 16. Furthermore, Giampa et al. (2017) suggested that the uplift of a shallow anchor causes failure to extend toward the ground surface, while the uplift of a deep anchor shows a more localized failure. The transition from "shallow" to "deep" failure is not distinct and is assumed to range from depth to diameter ratios of 4 to 10. In this study, the ratio of depth to wing diameter is approximately 5 to 7. However, as the area of the wing plate is small, it is assumed that uplift of wing plate causes local failure.

In the model proposed by Kanatani and Akino, the ultimate wing resistance R_{wtmax} is given as the sum of T_{AB}, T_{BC} and T_{ABCD} ($R_{wtmax} = T_{AB} + T_{BC} + T_{ABCD}$). T_{AB}, T_{BC}, T_{ABCD} represent shear force acting on surface S_{AB}, overburden load acting on surface S_{BC}, and dead load of soil mass ABCD, respectively. In the model, it is assumed that S_{BC} draws a logarithmic spiral. in Figure 16, α and α' for a logarithmic spiral are assumed as the follows:

$$\alpha = \frac{\pi}{4} + \frac{\phi_d'}{2} \tag{3}$$

$$\alpha' = \frac{\pi}{2} - \phi_d' \tag{4}$$

where, ϕ_d' is an internal frictional angle. T_{AB} is defied as the following equation:

$$T_{AB} = 2\pi b \cdot L \cdot \tau_{AB} \tag{5}$$

where, τ_{AB} is the shear stress acting on surface S_{AB}. L and b are defined as follows:

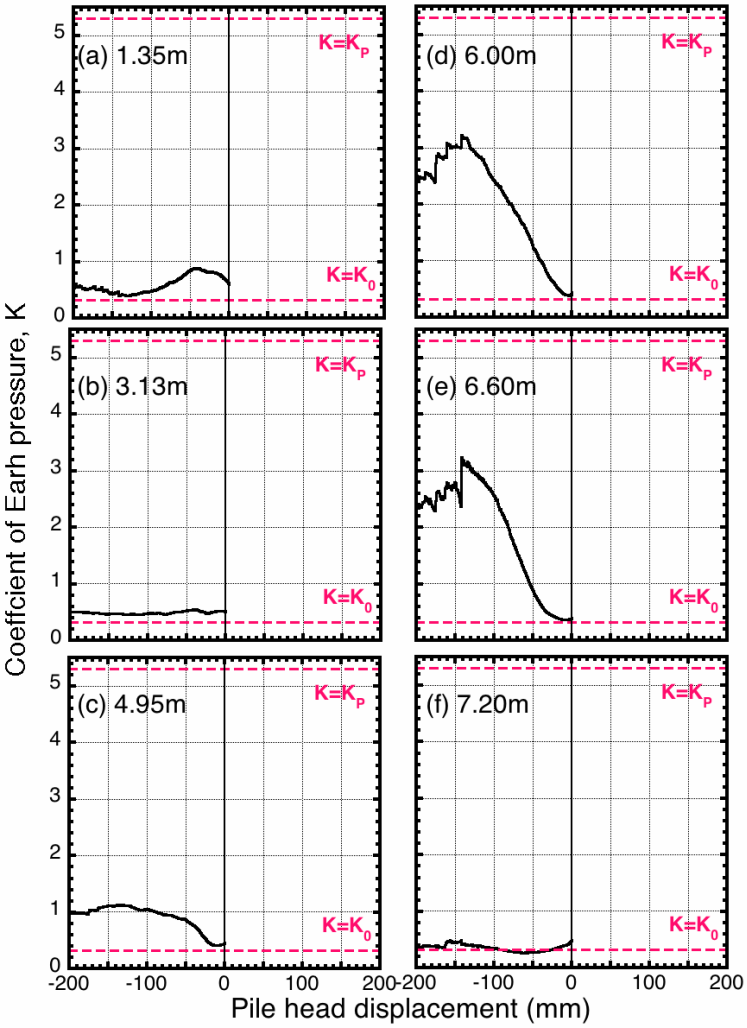

Figure 15. Relationship between earth pressure coefficient and pile head displacement

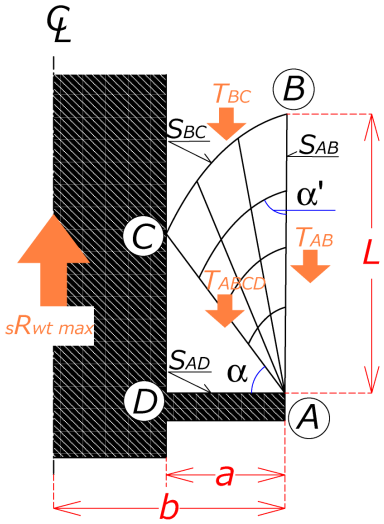

Figure 16. Ultimate wing resistance

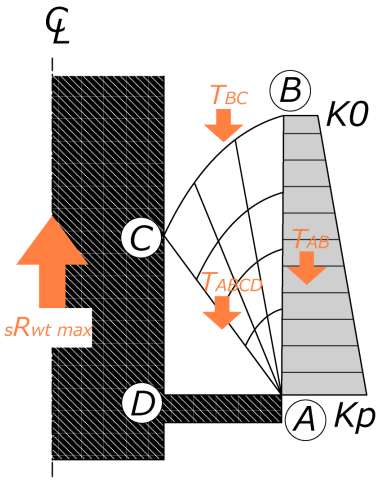

Figure 17. Coefficient of earth pressure above wing plate

$$L = \frac{a}{\cos\alpha} e^{\tan\phi_d' \cdot (\frac{\pi}{4} - \frac{\phi_d'}{2})} \quad (6)$$

$$a = (D_w - D)/2 \quad (7)$$

$$b = D_w/2 \quad (8)$$

where, D and D_w are diameters of the shaft and a wing, respectively.

In this study, to calculate the wing resistance in the centrifuge tests, τ_{AB} was estimated based on the observed coefficient earth pressure. As shown in Figure 17, the coefficient of earth pressure above the wing plate is assumed to change from passive state (K_P) to that at rest (K_0) along surface S_{AB}. Then, shear stress τ_{AB} is given as follows:

$$\tau_{AB} = \gamma \frac{(z_A \cdot K_p + z_B \cdot K_0)}{2} \tan\phi_d' \quad (9)$$

in which z_A and z_B are depths for points A and B in Figure 17 and γ is the unit weight of soil. The substitution of Equations (6)-(9) in Equation (5) gives T_{AB}. The sum of T_{BC} and T_{ABCD} is defined as the weight of the soil above the wing plate, as shown in Equation (10).

$$T_{BC} + T_{ABCD} = \pi(b^2 - (b-a)^2) \cdot \gamma \cdot z_A \quad (10)$$

Figure 18 shows the relation between the observed and estimated wing resistances through open symbols. In wing-resistance estimation, the frictional angle of soil is assumed to be 43°. The observed values are larger than the estimated values. This is because, in this study, the wing resistance was estimated from the difference between the axial forces observed at strain gauge SG7 and pile tip. Namely, the observed wing resistance includes the shaft friction acting on a section above the wing plate to the point of SG7. Then, the wing resistance is revised with considering the shaft friction acting on the abovementioned section and is shown as closed symbols. The shaft friction of the abovementioned section is estimated from that of the neighboring depth, as the shaft friction depends on depth.

The revised wing resistance is generally in agreement with the estimated resistance, suggesting that the model, in which it is assumed that the coefficient of earth pressure above a wing plate changes from at rest to passive state, is promising for wing-resistance estimation. In this study, the uplift of the wing plate was assumed to cause local failure, and then more discussion on failure modes is needed.

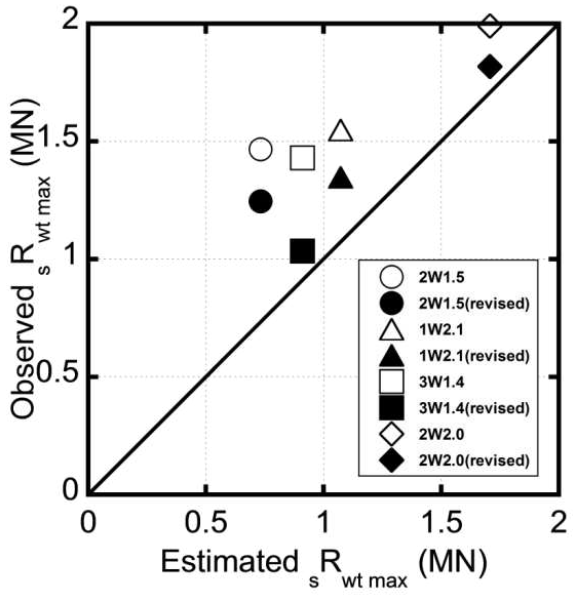

Figure 18. Relationship between estimated and observed wing resistances

5 CONCLUSIONS

Vertical loading tests were conducted under a displacement-controlled condition on piles with a wing plate. The results provide the following conclusions:

1) After reaching its ultimate value during cyclic loading, the shaft friction decreases to approximately 50 % in compression and to approximately 20 % in tension compared with those in monotonic loading with the same displacements.

2) Wing piles have high compression and tension resistances. With increasing displacement amplitude and the number of cycles, the uplift resistance of wing piles with a wing ratio (ratio of wing diameter to pile diameter) of approximately 1.5 decreases significantly, whereas that of wing piles with a wing ratio of approximately 2.0 does not show significant reduction.

3) The estimated wing resistance is generally in agreement with the observed resistance, suggesting that the model, in which the coefficient of earth pressure above a wing plate is assumed to change from at rest to passive state, is promising for wing-resistance estimation.

The vertical loading tests described in this study were conducted on reduced scale models, in which some conditions were different from real condition, for example the end condition and installation method. Therefore, the results should be carefully compared with those of field tests as well as those obtained in the previous studies.

References

Giampa, J. R., Bradshaw, A. S. and Schneider, J. A. 2017. Influence of dilation angle on drained shallow circular anchor uplift capacity, *International Journal of Geomechanics,* ASCE, 17(2).

Kanatani, Y. and Akino N. 1983. Ultimate uplift resistance of deep foundation with enlarged base, *Proceedings of Annual Meeting of Architectural Institute of Japan*, 2673-2674 (in Japanese).

Schneider, J. A., Xu, X. and Lehane, B. M. 2008. Database assessment of CPT-based design methods for axial capacity of driven piles siliceous sands, *Journal of Geotechnical and Geoenvironmental Engineering,* ASCE, 134(9): 1227-1244.

Suzuki, H., Inamura, K., Tokimatsu, K., Wada, M, and Mano, H. 2013. Estimation of bearing capacity and pull-out resistance of a pile with or without a wing plate in alternately cyclic loading based on centrifugal model tests, *Proceedings of 10th International Conference on Urban Earthquake Engineering*.

Suzuki, H., Urabe, K., Tokimatsu K, and Asaka, Y. 2014. Experimental investigation on pull-out resistance of a pile with a wing plate in alternately cyclic loading. P*roceedings of 10th National Conference on Earthquake Engineering*.

Tsuha, C. H. C, Foray, P. Y., Jardine, R.J., Yang, Z.X, Silva, M. and Rimoy, S. 2012, Bahavior of displacement piles in sand under cyclic axial loading, *Soils and Foundations*, JGS, 52(3): 393-410.

Urabe, K., Tokimatsu, K., Suzuki, H. and Asaka, Y. 2015. Bearing capacity and pull-out resistance of wing piles during cyclic vertical loading, *Proceedings of the 6th International Conference on Earthquake Geotechnical Engineering*.

White, D.J. and Lehane, B.M. 2004. Friction fatigue on displacement piles in sand, Geotechnique, 54(10): 645-658.